Indian Journal of Engineering & Materials Sciences
Vol. 31, April 2024, pp. 182-192
DOI: 10.56042/ijems.v31i2.6841

Numerical investigation on Williamson nanoflow past a cylinder imbedded in an absorbent media with energy source/sink: Keller Box simulation

B Vinoth Kumar and T Poornima*

Department of Mathematics, School of Advanced Sciences,
Vellore Institute of Technology, Vellore 632014, India

Received: 17 April 2023; Accepted: 05 October 2023

This article investigates the nanoflow with base fluid as Williamson along a circular cylinder incorporating non-linear energy generation/absorption embedded in a porous media. The obeying boundary layer balances for flow field, energy and diffusion transfer are modelled under Boussinesq approximation. Dimensional partial differential equations have been converted to dimensionless partial differential equations by adaptable non-similar variables. Obtained partial differential equations have been handled by Thomas algorithm of solving partial differential equations. It is finite difference method usually named as Keller box method. Varied fluid parameters like Williamson, porous, radiation, heat source/sink, buoyancy ratio and inertial force parameter characteristics on the flow field are graphically illustrated. Additionally, shear friction, heat and mass transfer rate have been estimated for the flow control parameters. Stream wise velocity improves, the skin friction coefficient decreases. As non-uniform heat generation parameter improves, the energy transfer rate and friction factor increase since more heat transfer from the wall have been absorbed by the fluid. Concentration rate near the cylinder wall decreases as energy producing is more in the fluid.

Keywords: Keller box method, Radiation, Williamson fluid, Soret and Dufour number, Forchheimer number, Heat source and sink

1 Introduction

Shear thinning fluids exhibits Williamson fluid model**.** This model has contained the minimum and maximum viscosities (μ_0, μ_∞).Williamson (1926) carried out experiments, clarified the characteristics of pseudoplastics and framed a model. More accurately than any other model, this one matches the experimental data for polymer solutions and particle suspensions. Hashim *et al.*[1] gave impactable dual solutions on the impact of Williamson nanoflow past a contracting cylinder. Shah *et al.*[2] discussed the case of thin film flow of Williamson radiative fluid flow. Asjad *et al.*[3] investigated the motile micromoth's impact on Williamson flow with activation energy. Ananth kumar *et al.*[4] worked on the influence of non-uniform energy production on a chemically reacting Williamson fluid flow. Megahed *et al.*[5] considered a continuously moving plate flowing Williamson dissipative flow. Abbas *et al.*[6] worked on a non-linear stretching surface flowing Williamson dissipative nanoflow imbedded in an absorbent media.

Heat transfer is essential in engineering and manufacturing. It's critical to manage heat in various applications, from large-scale systems like reactors and spaceships to tiny electronic devices. Researchers have extensively studied heat transfer properties[7-12].The impact of thermal radiation on fluids containing nanoparticles focussed by Kho *et al.*[13]. Other studies explored energy transfer in fluids with special properties, including Williamson fluids with suspended particles by Ganesh kumar *et al.*[14]. Williamson fluids with radiation and dissipation was Megahed *et al.*[15], and three-dimensional stretchable Williamson fluids under radiation Moorthy and Pallavarapu *et al.*[16]. Saravana *et al.*[17] further investigated these fluids considering the effects of diffusion and radiation.

Fluids within porous materials play a vital role in many applications. These materials, like sponges or foams, can be found in processes like blending polymers and even lubrication. Notably, sodium, a non-Newtonian fluid, finds use in batch mixers within porous media. Hamdan *et al.*[18] investigated magnetohydrodynamic (MHD) flow within a porous medium, like the work of Christian *et al.*[19]. MHD flow involves electrically conducting fluids interacting with magnetic fields. Acharya *et al.*[20] focused on a porous plate embedded in an absorbent material, likely studying fluid absorption properties. Veera *et al.*[21] analysed fluid flow within a semi-infinite strip placed in a porous medium. Raghunath *et al.*[22]

*Corresponding author (E-mail: poornima.t@vit.ac.in)

examined the effects of energy and mass transfer within a permeable medium located between plates. Mishra *et al.*[23] explored the influence of heat sources and radiation on a micropolar fluid flow within a non-Darcy porous medium. Micropolar fluids exhibit both viscous and rotational characteristics, and non-Darcy media deviate from the standard Darcy's Law for fluid flow in porous materials.

Energy generation or absorption is a critical aspect of energy and mass transfer in boundary layer theory. Understanding heat transfer is crucial in various applications, including building design, computer chip cooling, and electronic circuits. In Magneto-hydrodynamics (MHD) flows, heat transfer becomes particularly important due to the significant temperature differences that can arise. Early works[24-26] discussed applications of this impact on diverse fields, potentially including neurobiology. Non-Newtonian with the impact of non-uniform heat source/sink was investigated by Konda *et al.*[27]. Jyotshna *et al.*[28] extended this study to Williamson gallium nitride nanoflow. The similar impacts on a stretched cylinder and porous medium was also examined[29-30] .

Thus, with above knowledge, no work is carried on Williamson nanoflow past a circular cylinder in the presence of non-linear energy generation/absorption embedded in a porous media. Such a model fluid flow problem is taken and solved by implicit Keller box method with non-similarity variables. This study practical applications such as pipelines and storage tank, industries reliant on precise fluid dynamics, like polymer and food processing, can benefit, mixing processes and improve heat transfer efficiency in reactors and tanks, circulation dynamics, arterial blockages.

1.1 Physical model of the Problem Statement

The geometry of the flow field is schematically depicted in Fig. 1. A time-independent, two-dimensional, Williamson nanoflow past a horizontal cylinder is taken for study problem. Flow field is under the involvement of unidirectional radiation and the flow field is prone to heat production/lost. The flow field could be well described in the way that the *x*-axis is the radial and *y*-axis is the tangential axis. Radius of the horizontal cylinder denoted by 'a' with gravity acting downwards. Since density variation is experienced, Boussinesq approximation holds then. Initially, the temperature and species concentration near the circular cylinder immersed with Williamson

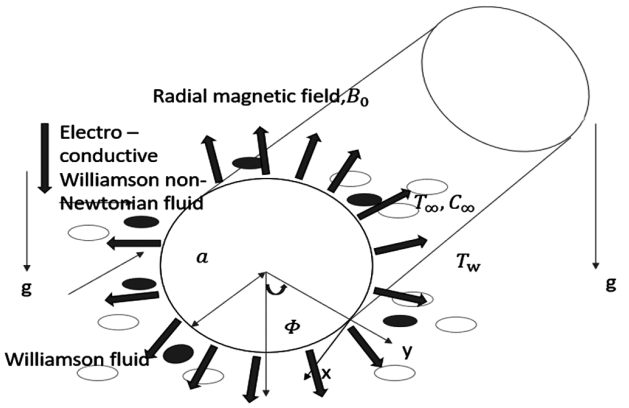

Fig. 1 — Coordinate system of geometry.

nanofluid are same. Then, it got raised to an instantaneous temperature (T_s>T_∞) and concentration (C_s> C_∞), maintained the same thereafter. Homogeneous porous medium is assumed with a permeability parameter (K). Under usual Boussinesq approximation, the leading boundary layer equations representing Williamson nanoflow from (*Rao et al.*[31]) are given as follows.

The constraint for our study is limited to the below.

$$y = 0 : v = u = 0, C = C_s, T = T_s,$$
$$y \to \infty : u \to 0, C \to C_\infty, T \to T_\infty. \quad ...(1)$$

The equations for mass continuity and the conservation of momentum, energy and concentration, can be written as follows (*Rao et al.*[31]):

$$u_x + u_y = 0 \quad ...(2)$$

$$\left[\begin{matrix}(1-C_\infty)\rho_{f\infty}\beta_t(T-T_\infty)- \\ (\rho_p-\rho_{f\infty})\beta_c(C-C_\infty)\end{matrix}\right] g\sin(x/a) + \nu u_{yy} + \sqrt{2}\nu\Gamma u_y u_{yy} - \frac{\mu}{K}u - \Gamma u^2 \Bigg) = u u_x + v u_y \quad ...(3)$$

$$\alpha_m \nabla^2 T + \tau\left[D_B C_y T_y + \left(\frac{D_T}{T_\infty}\right)T_y^2\right] - \frac{1}{\rho c_p}Q_y + q''' = uT_x + vT_y \quad ..(4)$$

$$D_B C_{yy} + \left(\frac{D_T}{T_\infty}\right)T_{yy} = uC_x + vC_y \quad ...(5)$$

Where:

$$q''' = \frac{ku_w}{x\nu}\left\{A^*\left(T_s - T_\infty\right)f' + B^*\left(T - T_\infty\right)\right\} \quad ...(6)$$

Rosseland heat approximation for optically thick fluids is:

$$Q = -\frac{4\sigma^*}{3k^*}\frac{\partial T^4}{\partial y} \quad ...(7)$$

Expanding T^4 in Eq. (7) as Taylor series about the point T_∞(as a linear function), we have

$$T^4 = -3T_\infty^4 + 4TT_\infty^3 \quad ...(8)$$

Substituting Eqns. (7)-(8) in Eq. (4) gives rise to the following form.

$$\left.\begin{aligned}&\tau\left[D_B C_y T_y + \left(\frac{D_T}{T_\infty}\right)T_y^2\right] + \frac{16\sigma^* T_\infty^3}{3k^*\rho c_p}T_{yy} + \alpha T_{yy}\\ &+\left[\frac{ku_w}{xv}\left(A^*\left(T_s - T_\infty\right)f' + B^*\left(T - T_\infty\right)\right)\right]\end{aligned}\right\} = uT_x + vT_y \quad ...(9)$$

Basing on stream function, definition $u = \frac{\partial\psi}{\partial y}$, $v = -\frac{\partial\psi}{\partial x}$ such that Eq. (1) satisfies trivially. The following non- similar variables introduced for transformation of leading PDEs to dimensionless.

$$a\xi = x,\ \ (Gr)^{-1/4}\, a\eta = y,\ \ f(\xi,\eta) = \frac{\psi}{v\xi}(Gr)^{-1/4},$$
$$(C_s - C_\infty)\phi(\xi,\eta) = C - C_\infty, (T_s - T_\infty)\theta(\xi,\eta) = T - T_\infty,$$
$$\alpha_m = \frac{k_m}{(\rho c)_f},\quad \tau = \frac{(\rho c)_p}{(\rho c)_f},\ Gr = \frac{(1-\phi_\infty)\rho_{f\infty} g\beta(T_s - T_\infty)a^3}{v^2}. \quad ...10)$$

Inserting Eq. (10) into Eq. (3), (9), (5), the transformed system of equations are derived as

$$f''' + (f + We\, f'')f'' - (1+\xi\Lambda)f'^2 + \frac{\sin\xi}{\xi}(\theta - Nr\phi) + \frac{1}{Da}f' = \xi\left(\frac{\partial f'}{\partial\xi}f' - \frac{\partial f}{\partial\xi}f''\right) \quad ...(11)$$

$$\left(1+\frac{4}{3F}\right)\frac{\theta''}{\Pr} + f\theta' + Nb\phi'\theta' + Nt\theta'^2 + (Af' + B\theta) = \xi\left(f'\frac{\partial\theta}{\partial\xi} - \theta'\frac{\partial f}{\partial\xi}\right) \quad ...(12)$$

$$\phi'' + Scf\phi' + \left(\frac{Nt}{Nb}\right)\theta'' = \xi\left(\phi_\xi f' - \xi f_\xi\phi'\right) \quad ...(13)$$

Associated constraints are:

$$\eta = 0 : f(\eta) = 0,\ f'(\eta) = 0,\ \phi(\eta) = 1, \theta(\eta) = 1,$$
$$\eta \to \infty : f'(\eta) \to 0, \phi(\eta) \to 0, \theta(\eta) \to 0. \quad ...(14)$$

The obsessive flow field quantities seen in above equations are:

$$\Lambda = \Gamma a;\ We = \frac{\sqrt{2}v\Gamma Gr^{3/4}}{a^2}; Nr = \frac{(\rho_p - \rho_{f\infty})(C_s - C_\infty)}{\rho_{f\infty}(1-C_\infty)\beta(T - T_\infty)};$$
$$Da = \frac{K}{Gr^{1/2}a^2};\ \Pr = v/\alpha_m;\ Sc = v/D_m\varepsilon; Nb = \tau\frac{D_B(C_s - C_\infty)}{v};$$
$$Nt = \tau\frac{D_T(T_s - T_\infty)}{vT_\infty}; F = \frac{Kk^*}{4\sigma^* T_\infty^3}. \quad ...(15)$$

Most influential quantities for engineering design like wall shear stress, energy and mass transfer rates, are presented here

$$C_f = Gr^{\frac{3}{4}}\xi f''(\xi,0)\left[1 + \frac{Wef''(\xi,0)}{2}\right];$$
$$Nu = -\theta'(\xi,0)Gr^{\frac{1}{4}}; Sh = -\phi'(\xi,0)Gr^{\frac{1}{4}} \quad ...(16)$$

2 Materials and Methods

2.1 Numerical analysis

The system of equations associated boundary conditions from Eq. (11) through (14) are assessed by Keller box (Keller, Herbert [33]) as this algorithm is unconditionally stable method with 2nd order precision. The Keller box method in computational fluid dynamics is a numerical approach used to solve partial differential equations that describe fluid flow phenomena. Keller box method offers a versatile numerical approach for solving fluid dynamics problems, particularly those featuring time-dependent behaviour or moving boundaries.

The following actions will be performed in this method:

Step 1: n^{th} order differential equations to n first order equations reduction.

Step 2: A central difference approach is used for discretization.

Step 3: Non-linear leading equations are linearized through Newton's technique.

Step 4: Tridiagonal matrices were formed and solved by LU decomposition method.

Step 1:

We took $f' = u; f'' = v; \theta' = t; \phi' = p$ then the reduced Eqs. (11)-(14) takes the below structure:

$$v' + fv - (1+\Lambda\xi)u^2 + We(vv') + \frac{\sin\xi}{\xi}\left[S - Nr(g)\right] - \frac{1}{Du} = \xi\left(uu_\xi - vf_\xi\right), \quad ...(17)$$

$$\frac{1}{\Pr}\left(1+\frac{4}{3F}\right)t' + ft + Nb(pt) + Nt(t^2) + Au + Bs = \xi\left(us_\xi - tf_\xi\right), \quad ...(18)$$

$$\frac{1}{Sc}p' + fp + \frac{1}{Sc}\left(\frac{Nt}{Nb}\right)t' = \xi\left(ug_\xi - pf_\xi\right). \quad ...(19)$$

Conditions turn up like

$$At\ \ \eta = 0:\quad f(\eta) = 0,\ u(\eta) = 0, g(\eta) = 1, s(\eta) = 1,$$

$$As\ \ \eta \to \infty:\ \ u(\eta) \to 0, g(\eta) \to 0, s(\eta) \to 0. \quad ...(20)$$

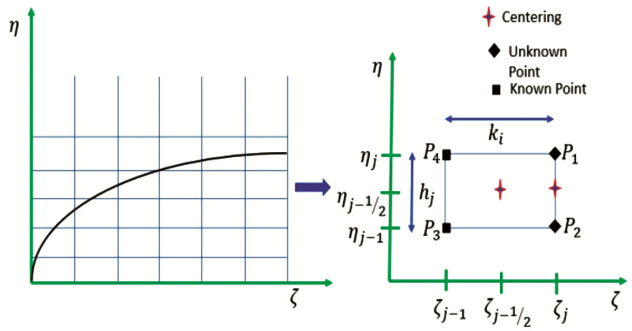

Fig. 2 — Keller box element and boundary layer mesh.

Step 2: Discretization of domain using central difference approach

The differences in $\xi-\eta$ computational grid is defined below (Fig. 2).

$$j=1,2,...,J:\eta_0=0,\ \eta_j=\eta_{j-1}+h_j,\ \eta_J\equiv\eta_\infty;$$
$$q=1,2,...,N:\xi^0=0,\ \xi^q=\xi^{q-1}+k_q. \quad ...(21)$$

where h_j, k_q - the heights along η-ξ directions, respectively. Few more definitions of differences are as follows.

$$\Psi_{j-1/2}^{n-1/2}=\frac{\left(\Psi_{j-1}^{n-1}+\Psi_j^{n-1}\Psi_j^n+\Psi_{j-1}^n\right)}{4}$$

$$\left(\frac{\partial\Psi}{\partial\eta}\right)_{j-\frac{1}{2}}^{n-\frac{1}{2}}=\frac{\left(\Psi_j^n+\Psi_j^{n-1}-\Psi_{j-1}^n-\Psi_{j-1}^{n-1}\right)}{2h_j}$$

$$\left(\frac{\partial\Psi}{\partial\xi}\right)_{j-\frac{1}{2}}^{n-\frac{1}{2}}=\frac{\left(\Psi_j^n+\Psi_j^{n-1}-\Psi_{j-1}^n-\Psi_{j-1}^{n-1}\right)}{2k_q} \quad ...(22)$$

At mid-point $\left(\eta_{j-1/2},\xi^n\right)$, the finite-difference approximation is as follows.

$$h_j^{-1}\left(f_j^n-f_{j-1}^n\right)=u_{j-1/2}^n;\ h_j^{-1}\left(u_j^n-u_{j-1}^n\right)=v_{j-1/2}^n$$
$$h_j^{-1}\left(\theta_j^n-\theta_{j-1}^n\right)=t_{j-1/2}^n;\ h_j^{-1}\left(\phi_j^n-\phi_{n-1}^n\right)=g_{j-1/2}^n \quad ...(23)$$

Introducing (22)- (23) in (17)-(19), we get

$$\left[1+\frac{Weh_j}{4}\left(v_{j-1}+v_j\right)\right]\left(v_j-v_{j-1}\right)+\left[\frac{(1+\alpha)h_j}{4}\left(f_{j-1}+f_j\right)-\frac{\alpha h_j}{2}f_{j-1/2}^{n-1}\right]\left(v_{j-1}+v_j\right)$$
$$-\frac{h_j}{4}(1+\Lambda\xi+\alpha)\left(u_j+u_{j-1}\right)^2+\frac{Bh_j}{2}\left(s_j+s_{j-1}\right)-\frac{Bh_j}{2}Nr\left(g_j+g_{j-1}\right)-\frac{h_j}{2Da}\left(u_j+u_{j-1}\right)+$$
$$\frac{\alpha h_j}{2}\left(f_j+f_{j-1}\right)v_{j-1/2}^{n-1}=-\left[R_1\right]_{j-1/2}^{n-1} \quad ...(24)$$

$$\left[\begin{matrix}\frac{(1+\alpha)h_j}{4}\left(f_{j-1}+f_j\right)-\frac{\alpha h_j}{2}f_{j-1/2}^{n-1}\\+\frac{Nbh_j}{4}\left(p_{j-1}+p_j\right)+\frac{Nth_j}{4}\left(t_{j-1}+t_j\right)\end{matrix}\right]\left(t_{j-1}+t_j\right)+\frac{\alpha h_j}{2}\left[s_{j-1/2}^{n-1}\left(u_j+u_{j-1}\right)-u_{j-1/2}^{n-1}\left(s_j+s_{j-1}\right)\right]$$
$$+\left[\frac{Ah_j}{2}-\frac{\alpha h_j}{4}\left(s_j+s_{j-1}\right)\right]\left(u_j+u_{j-1}\right)+\alpha t_{j-1/2}^{n-1}\left(f_{j-1}+f_j\right)+\frac{Bh_j}{2}\left(s_{j-1}+s_j\right)$$
$$-\frac{1}{\Pr}\left(1+\frac{4}{3F}\right)\left(t_{j-1}-t_j\right)=\left[R_2\right]_{J-\frac{1}{2}}^{n-1} \quad (25)$$

$$\frac{1}{\Pr}\left(p_j-p_{j-1}\right)+\left(p_j+p_{j-1}\right)\left[\begin{matrix}\frac{h_j(1+\alpha)}{4}\left(f_{j-1}+f_j\right)\\-\frac{\alpha h_j}{2}f_{j-\frac{1}{2}}^{n-1}\end{matrix}\right]+\frac{1}{Sc}\left(\frac{Nt}{Nb}\right)\left(t_j-t_{j-1}\right)+\frac{\alpha h_j}{2}g_{j-1/2}^{n-1}\left(u_j+u_{j-1}\right)$$
$$-\left[\frac{\alpha h_j}{2}u_{j-1/2}^{n-1}+\frac{\alpha h_j}{4}\left(u_j+u_{j-1}\right)\right]\left(g_j+g_{j-1}\right)+\frac{\alpha h_j}{2}p_{j-1/2}^{n-1}\left(f_{j-1}+f_j\right)=\left[R_3\right]_{j-1/2}^{n-1} \quad ...(26)$$

where R_i's are weighted residuals with

$$\alpha=\frac{\xi^{n-1/2}}{k_n},B=\frac{\sin\xi}{\xi}$$

The boundary conditions are as follows.

$$p_0^n=1,\ s_0^n=1,u_0^n=0,\ f_0^n=0,$$
$$p_J^n=0,s_J^n=0,u_J^n=0. \quad ...(27)$$

Step 3: Through Newton's approach, linearization is made

If we assume all values *f, u, v, s, t, p at* $\left(\ \right)_j^{n-1}$ levels are provided $\forall j\in(0,J)$ then Eqns. (21)-(24) will be a system of $7(j+1)$ for $j=J$ equations with same quantity of unknowns. Through Newton's approach the equations are quasi-linearized with known $[R_1],[R_2],[R_3]$. For quasi-linearization, we introduce the following equality for all variables *f, u, v, s, p, t*:

$$\left(\ \right)_j^{(i+1)}=\sum\left(\ \right)_j^{(i)}+\delta\left(\ \right)_j^{(i)} \quad ...(28)$$

$$\left[R_1\right]_{j-1/2}^{n-1}=-\left(\frac{v_j^{n-1}-v_{j-1}^{n-1}}{h_j}\right)-(1-\alpha)(fv)_{j-\frac{1}{2}}^{n-1}+(1+\Lambda\xi-\alpha)\left(u_{j-1/2}^{n-1}\right)^2-Wev_{j-1}v'_{j-1/2}$$
$$-B\left[s_{j-1/2}^{n-1}-Nr\left(g_{j-1/2}^{n-1}\right)\right]+\frac{1}{Da}u_{j-1/2}^{n-1} \quad ...(29)$$

$$\left[R_2\right]_{J-1/2}^{n-1}=-\frac{1}{\Pr}\left(1+\frac{4}{3F}\right)\left(\frac{t_j^{n-1}-t_{j-1}^{n-1}}{h_j}\right)-(1-\alpha)(ft)_{j-1/2}^{n-1}-Nb(pt)_{j-1/2}^{n-1}$$
$$-Nt\left(u_{j-1/2}^{n-1}\right)^2-Au_{j-1/2}^{n-1}-Bs_{j-1/2}^{n-1}-\alpha(us)_{j-1/2}^{n-1} \quad ...(30)$$

$$[R_3]_{j-1/2}^{n-1} = -\frac{1}{Sc}\left(\frac{p_j^{n-1}-p_{j-1}^{n-1}}{h_j}\right)-(1-\alpha)(fp)_{j-1}^{n-1}-\alpha(ug)_{j-1/2}^{n-1}-\frac{1}{Sc}\left(\frac{Nt}{Nb}\right)\left(\frac{t_j^{n-1}-t_{j-1}^{n-1}}{h_j}\right)$$

...(31)

The other set of residuals $r_i's$ with constants a_i's, b_i' s, c_i' s can also be derived at *j- th,* position in terms of $j - ½$.

Step 4: The linearized system of equations is transformed to block tridiagonal structure, solved by the Thomas algorithm[33]. Block matrix system represent the entire linearized system, where each component of the coefficient matrix. An efficient Keller-box method is employed to assess the system. Number of grids used has an impact on the numerical output. MATLAB software is used to get the mesh independence. Larger number of trials and more mesh points are included along η direction whilst lesser number is taken along tangential direction.

3 Results and Discussion

The highly coupled system solved employing Keller box algorithm. Computations are carried through MATLAB software. The impact of various pertinent physical parameters on the flow field and engineering quantities are explained through figures 3-46. Here maximum value of $(\eta, \xi) = (10,1)$is taken for which the boundary conditions are satisfied. Throughout the calculations, the parametric values are chosen for study as $\xi = 1.0, Nt = 0.1, Nr = 0.1, \Lambda = 0.5, Da = 10,$ $\Pr = 0.7, Sc = 0.6, A = 0.1 = B.$ The range of parameters are $0 \le Nt \le 1.5,\ 0.01 \le Nb \le 4.0, 0 \le Nr \le 0.6,$ $0.0 \le We \le 0.3, 0 \le A, B \le 0.4,\ 0 \le \Lambda \le 1.5, 0 \le F \le 1.0$.

Table 1 describes the comparison of our computational results with Rao *et al.*[31] and Prasad *et al.*[32] for the reduced cases i.e., absence of Soret, Du four buoyancy ratio and heat source /sink and found a good agreement.

Figure. 3(a-c) show the deviations in momentum, energy, and species with varied Soret number (Nt). Augmenting Soret number($Nt = 0.0,0.5,1.0,1.5$)

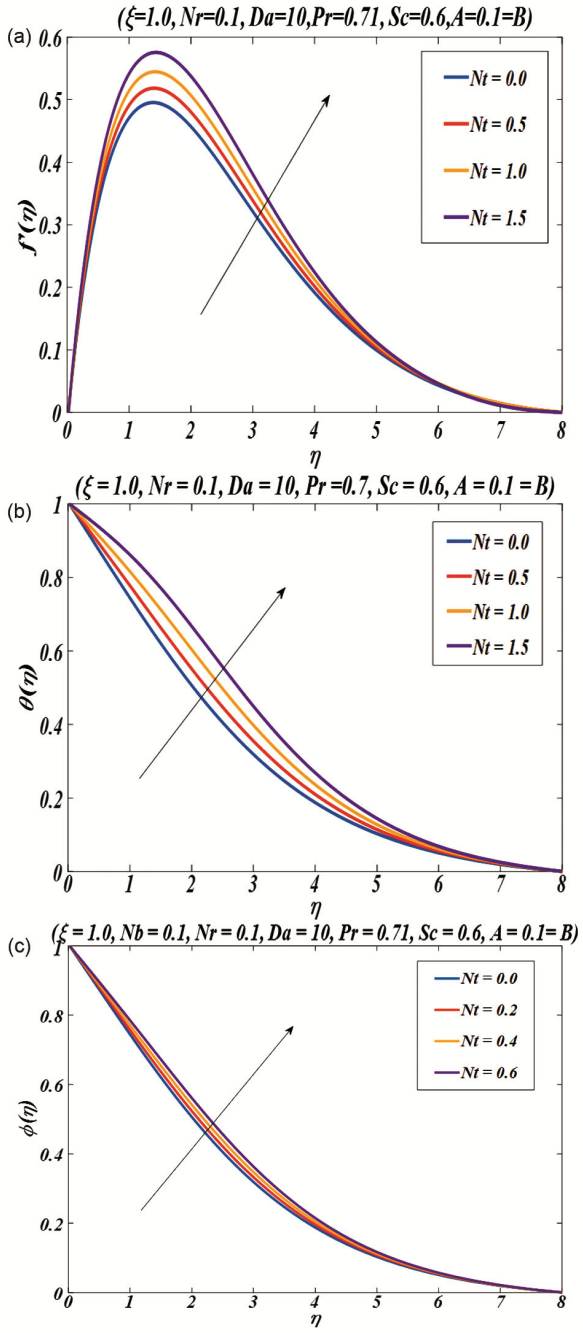

Fig. 3 — (Nt=0.0,0.5,1.0,1.5) influence on (a) velocity, (b) temperature, and (c) concentration profiles.

Table 1 — Values of the shear stress near cylinder surface for different (Pr) Values

ξ	$Pr = 5$			$Pr = 0.72$		
	Prasad *et al*. [32]	Rao *et al*. [31]	Our results	Prasad *et al*. [32]	Rao *et al*. [31]	Our results
0	0.0000	0.0000	0.0000	0.00000	0.0000	0.0000
0.8	0.567	0.569	0.5678	1.157	1.159	1.1589
1.2	0.784	0.784	0.7765	1.598	1.600	1.6012
2.8	0.625	0.626	0.6261	1.400	1.402	1.4026
3.14	0.225	0.228	0.2307	0.702	0.713	0.7094

randomizes the movement of nanoparticles which affects the viscosity of the flow by decelerating the momentum boundary layer thickness. So, falling velocity profiles are seen. Random diffusion in nanoparticles enhances the temperature of the flow naturally, hence, there finds a rising profiles of species diffusion and energy of the flow. Pedesis is parameterized as Dufour number (Nb=1,2,3,4), with its decrement energy difference is observed within fluid and surface, naturally heat transfers more inside the fluid which affects the fluid's viscosity. Thus, it is found that momentum boundary layer is higher than thermal and concentration boundary layer thickness. Hence, velocity swifts up, but energy and concentration diffusion are low (Fig. 4(a-c). Flow motion swifts down as the buoyancy ratio (Nr=0.0,0.2,0.4,0.6) escalates. The buoyancy forces offer an obstruction by nature which restricts the movement of fluid flow. Temperature also rises quickly, and species diffusion boundary layer also thickens. So, the velocity of the nanoflow decelerates and concentration boundary layer also de-thickens (Figs 5(a-c)). Forchheimer parameter (Λ) effect on three flow field quantities is presented in Figs 6(a-b). Inertial forces act against the viscosity of fluid, so the motion of the flow is resisted. Momentum boundary layer thickness reduces and thereby decelerating the flow motion. It is found that deceleration in the fluid motion, increases the energy inside the nanoflow and boosts the concentration diffusion.

Role of the viscoelastic parameter (We=0.0, 0.1,0.2,0.3) on the nanoflow quantities is assessed in Figs 7(a-c). Augmenting Weissenberg number decelerates the motion of the flow since We accelerates the elastic forces. In this case viscosity becomes more significant which creates resistance to the fluid flow. Figures 7(b-c) show the declining profiles of energy and concentration. Figures 8(a-f) represents the effect of variable heat source parameter on flow field quantities. Heat source induces heat inside the nanoflow which upsurges the viscidness of the flow, thus an escalation in the momentum of the flow and energy too enhances. But the concentration profiles are declining. Temperature inside the flow rises quickly by reducing the viscosity of the flow, loosens the diffusion of particles as the intensity of radiation enhances. So, the velocity ($F = 0.1,0.3,0.6,1.0$) of the nanoflow decelerates and concentration boundary layer also de-thickens [(Figs 9(a-c)].

Engineering quantities are portrayed in Figs (10-13). Non-uniform heat production on different engineering

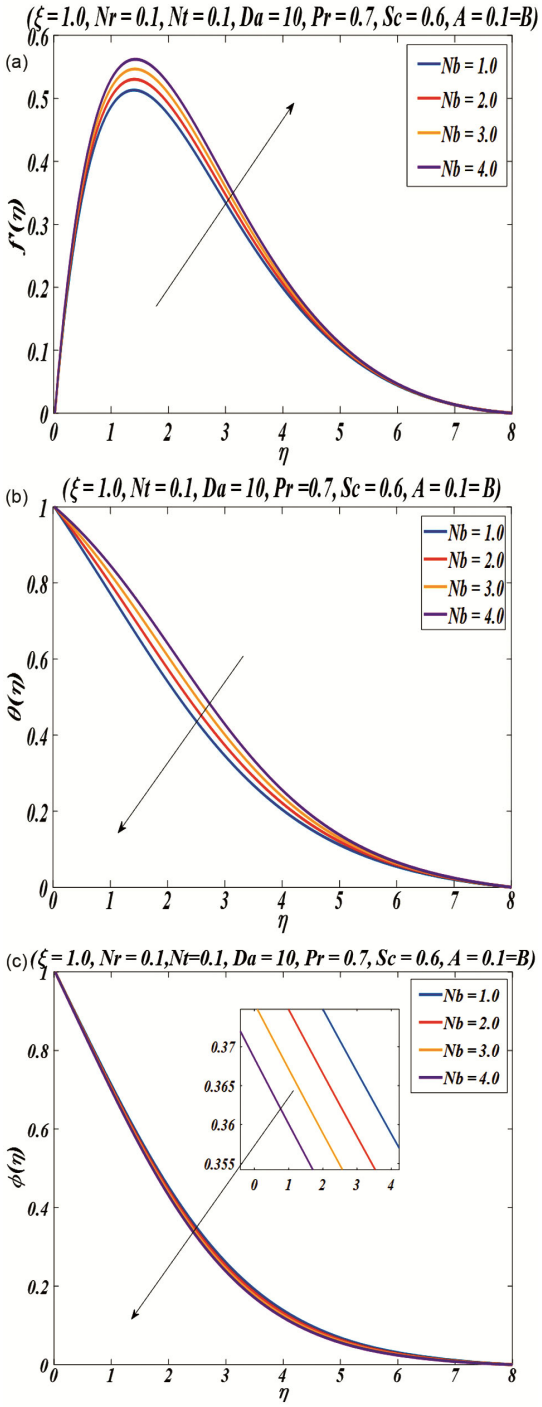

Fig. 4 — (Nb=*1.0,2.0,3.0,4.0*) shows effect on the flow field (a) velocity, (b) temperature, and c) concentration.

quantities is depicted in Fig. 10(a-e). Here the physical quantities are drawn against the stream wise velocity. Augmenting ξ makes all engineering quantities to decline except the skin friction coefficient, where the profiles start from 0 and swifts approximately to a

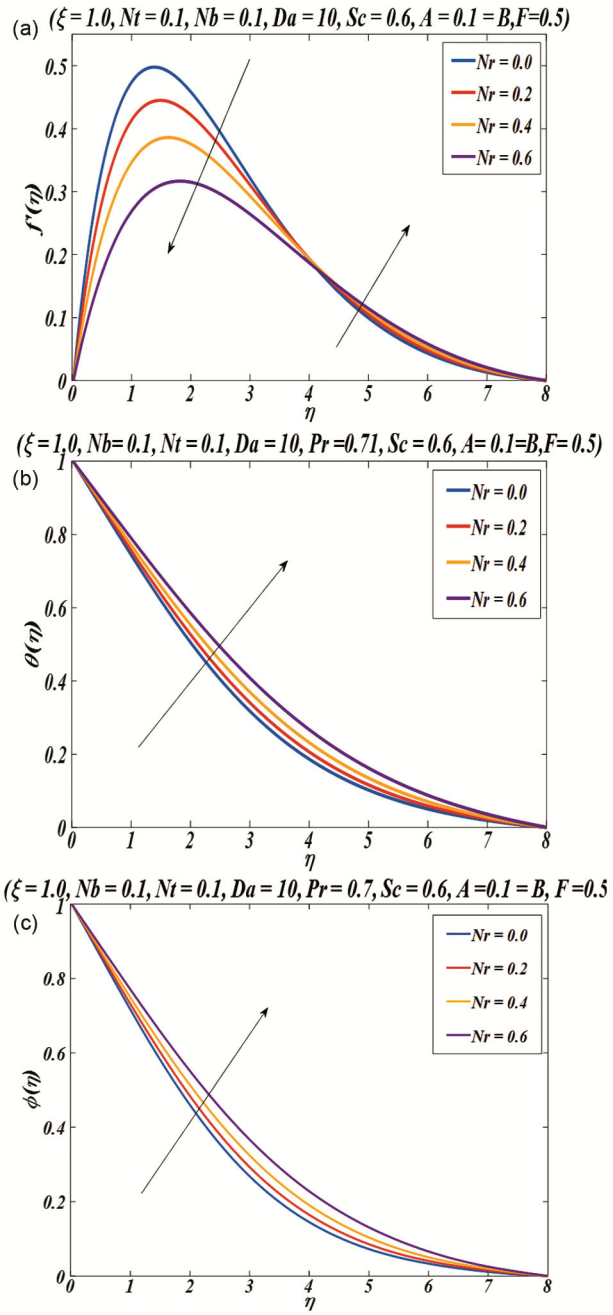

Fig. 5 — (*Nr=0.0,0.2,0.4,0.6*) shows effect on the flow field (a) velocity, (b) temperature, and c) concentration.

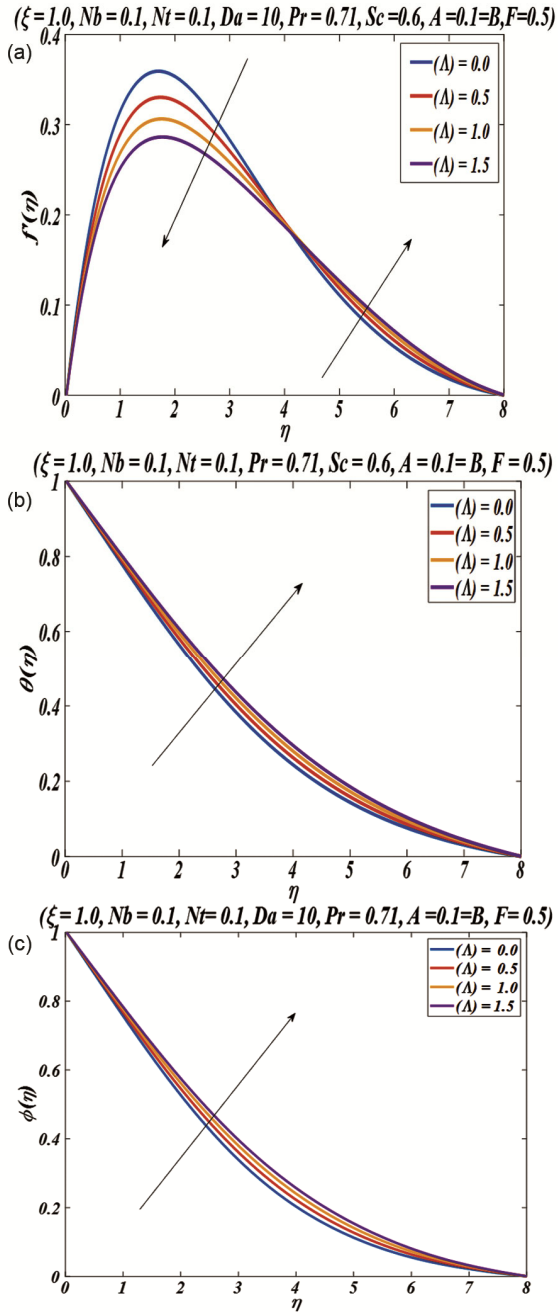

Fig. 6 — (Λ=0.0,0.5,1.0,1.5) shows effect on the flow field (a) velocity, (b) temperature, and c) concentration.

highest value 1 and then falls. As the energy production parameter escalates, shear stress near the wall surface rises in the direction of stream-wise velocity function. Similar way, heat transfer also enhances as *A* improves. The same phenomenon is observed in both friction factor and energy transfer rate. Whilst the other parameter of energy generation parameter (*A* and *B*=0.0,0. 1,0.2,0.3) shows an escalating tendency in friction coefficient but the heat transfer rate drops as heat transfers from the wall surface to fluid rising the temperature inside the nanoflow instead wall. Effect of energy source parameter (*A*, *B*) on the cylinder surface shear factor, heat transfer and species transfer rate as the intensity of radiation parameter increases, friction on the wall increases since there finds an expanding momentum boundary layer thickness.

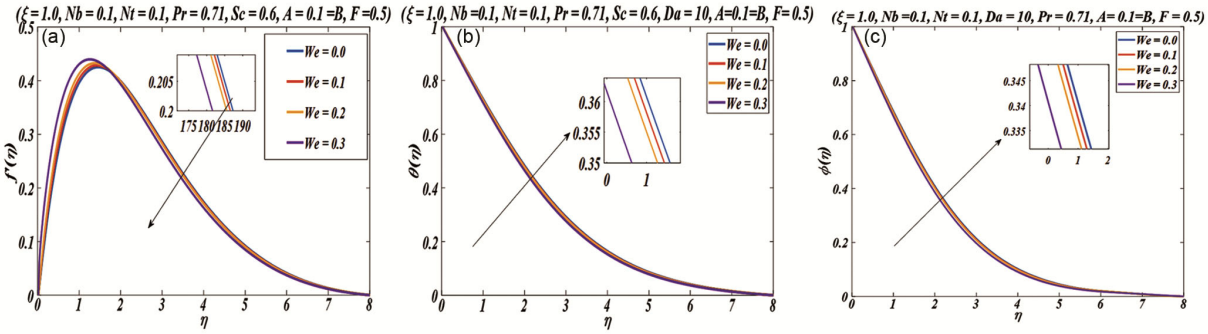

Fig. 7(a-c) — (*We=0.0,0.1,0.2,0.3*) shows effect on the flow field (a) Velocity, (b) temperature, and (c) concentration.

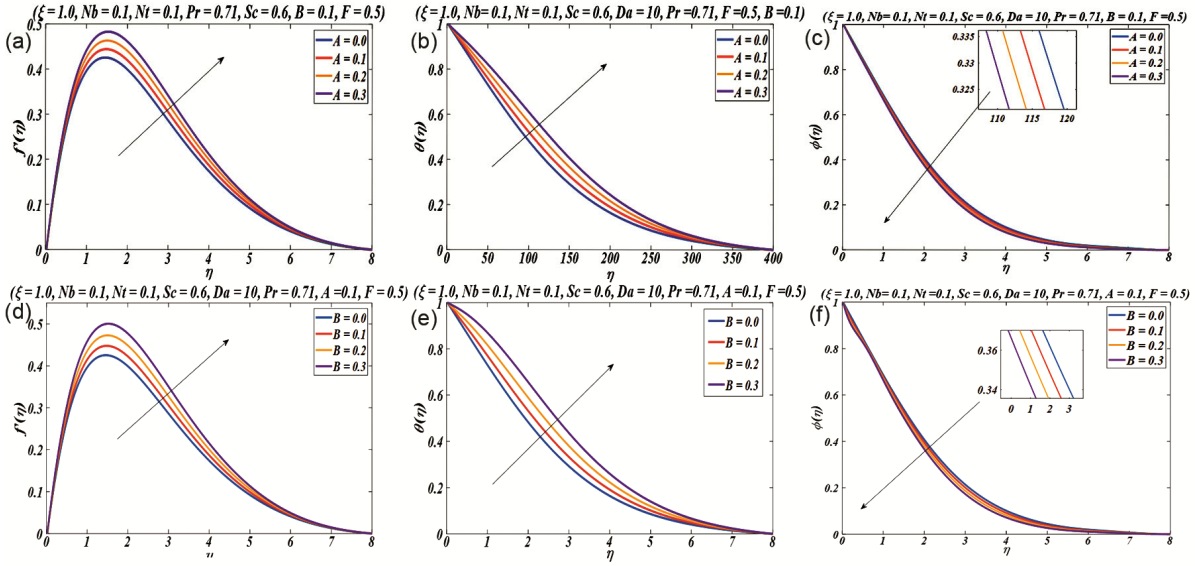

Figs. 8(a-f) — (*A and B=0.0,0.1,0.2,0.3*) shows effect on the flow field Velocity, temperature, concentration.

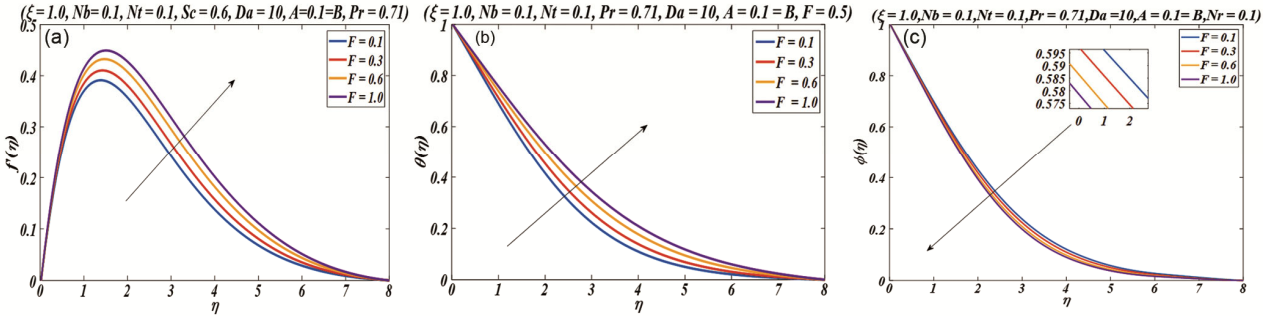

Fig. 9(a-c) — (*F*=0.1,0.3,0.6,1.0) shows effect on the flow field (a) Velocity, (b) temperature, and (c) concentration.

Figures. 11(a-c) shows the radiation impact on the surface shear factor, energy, and species rate of transfer. Radiation is denoted by *F,* the values of radiation parameter for (*F* =0.1,0.3,0.6,1.0) and the result is skin friction is increasing, Nusselt number is decreasing and Sherwood number also increasing. Due to friction near wall causes more heat transfer from wall to nanoflow, thus rate of heat transfer decreases as radiation intensifies. Inertial parameter also has a significant role in this study. It cools the system by transferring more heat and reduces the friction near the wall. Figure. 12(a) depicts a falling profile of diffusion rate as the stream wise velocity augments, while an opposite trended profile is seen as heat source enhances. As the radiation parameter rises, concentration rate diminution is seen (Fig.12(b)). Sherwood number

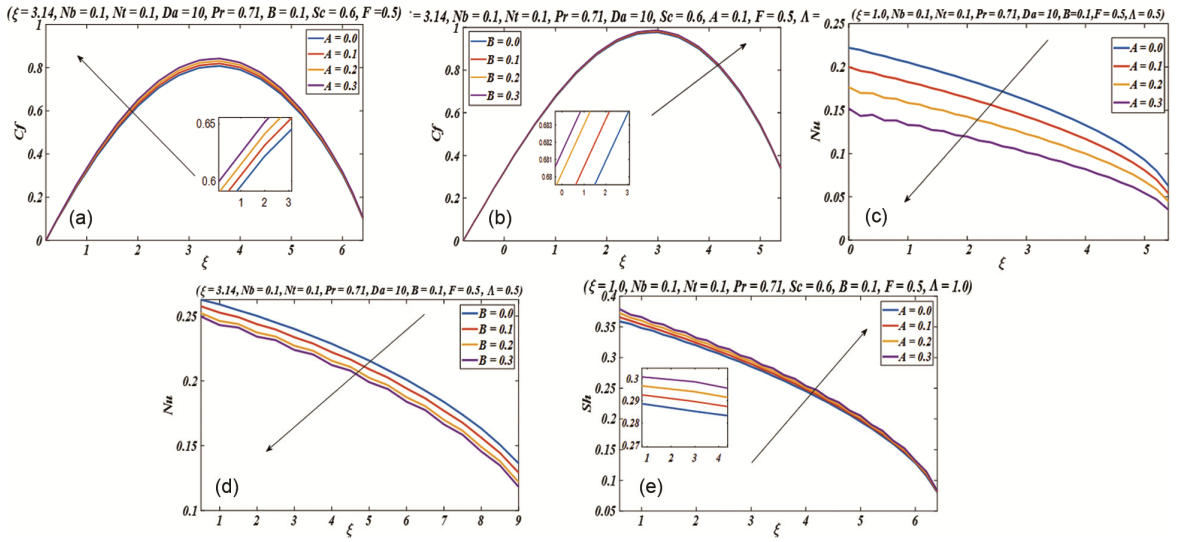

Fig. 10 — Effect of space (A) and time (B) dependent energy source parameter on Wall shear stress, (a-b) Nusselt number and 10(c-e) Sherwood number.

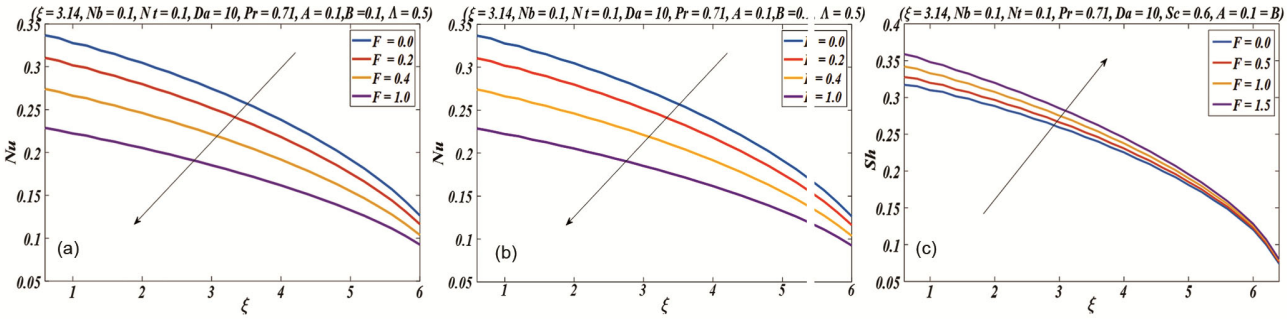

Fig. 11 — Effect of radiation parameter on Wall shear stress (a) Nusselt number, (b-c) Sherwood number.

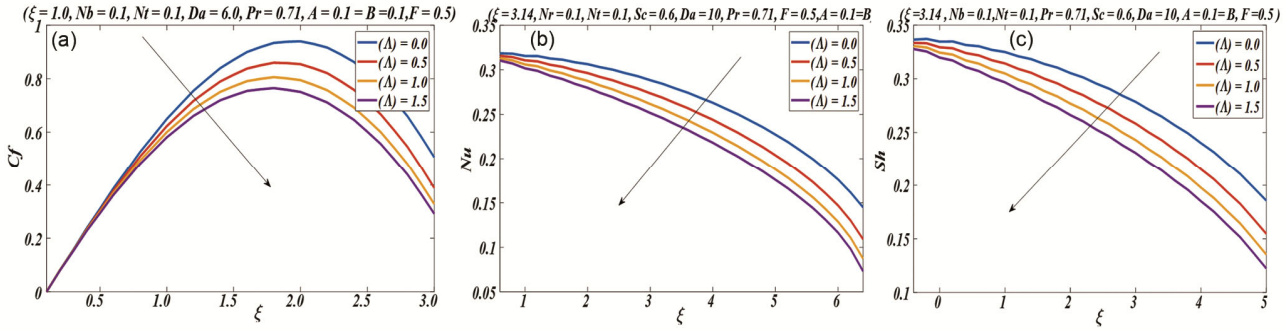

Fig. 12 — Influence on For chheimer parameter on skin friction coefficient (a) heat transfer rate ,(b) and (c) mass transfer rate.

declines as For chheimer parameter improves which is described in Fig.12(c).

Figures 13(a-b)show the effect of *(We)* parameter on skin friction coefficient, Nusselt number and Sherwood number. The values of Weissenberg number (*We*=0.0, 0.1, 0.2, 0.3) and the result is all the three profiles are increasing.

Figures 14 (a-f) are showing the streamlines for (*We* = 0.0, 0.2) parameter, (*Nr*= 0.2,0.4) parameter and (Λ = 1.0,2.0) parameter. Figures 14(a-b) show the *We* streamlines and figs. 14(c-d) show the *Nr* impacted streamlines. Figures 14(e-f) show the (Λ) parameter. streamline graphs are a fundamental tool in fluid dynamics, illustrating the trajectory of fluid particles

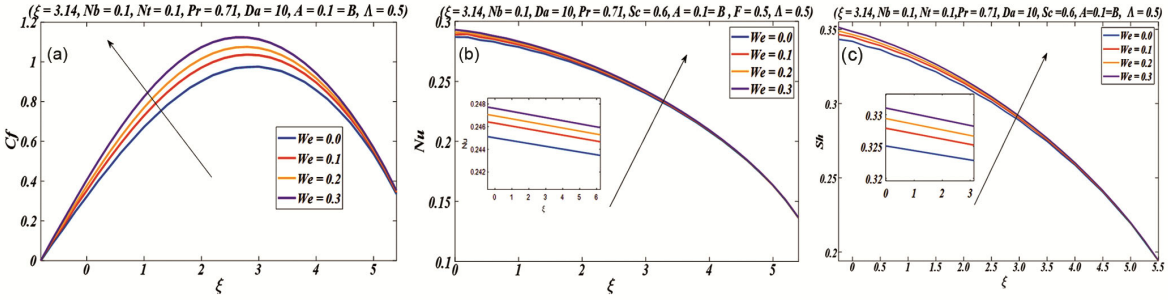

Fig. 13 — Influence on Weissenberg number on skin friction coefficient (a) heat transfer rate, (b), and (c) mass transfer rate.

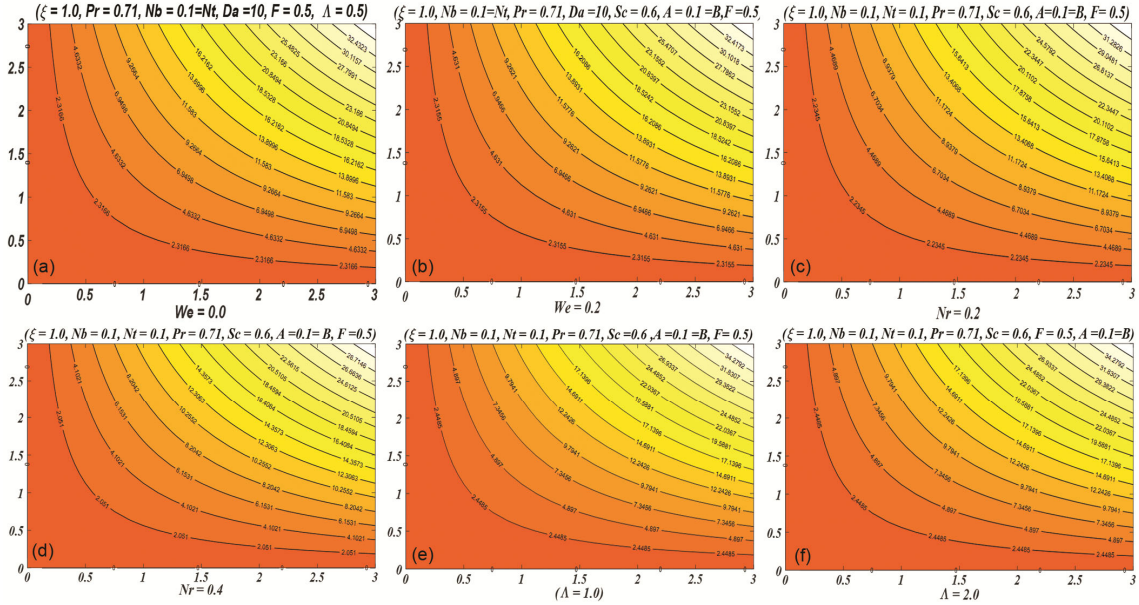

Fig. 14 — Streamlines indicating particle path for different Weissenberg number (a) *We* =0.0, (b) *We* =2.0, (c) *Nr* =0.2, (d) *Nr* =0.4, (e) Λ=1.0, and (f) Λ=2.0) is portrayed.

as they move within a flow field. These graphs consist of imaginary lines called streamlines, which represent the path a particle would follow at any given point in the flow. They are tangent to the velocity vector of the fluid, providing insights into the direction and speed of the flow at different locations. By observing the density and pattern of streamlines, researchers can analyse phenomena such as turbulence, stagnation points, and variations in flow velocity. Streamline graphs find applications across various fields, including engineering, meteorology, and oceanography, where they help predict and understand fluid behaviour in complex systems like airflow around objects or water currents in natural environments.

4 Conclusion

A free convective laminar incompressible nanoflow immersed in non-Darcy absorbent media along a horizontal circular cylinder is investigated in this paper. Incorporated radiation and time and space dependent heat generation gives a new dimension to the problem. Problem solved by an efficient finite-difference Thomas algorithm. The below conclusions can be drawn:

- Boosting Brownian motion parameter decelerates the fluid motion.
- As Soret number increases, both energy and diffusion rate enhance.
- Improving thermophoresis accelerates the fluid velocity but decreases energy as well as species concentration.
- Incrementing buoyancy ratio parameter, swifts down the momentum, whereas increases the temperature and concentration of the flow.
- Inertial force increases momentum boundary layer expands than thermal and concentration.
- Non-uniform energy generation parameter (*A*) improvement decreases the diffusion rate

but increases the momentum and energy inside the flow.

- Impact of (B) energy production is significant on velocity and temperature of nanoflow. But an opposite phenomenon is observed in concentration.
- Near the wall of the cylinder, the species diffusion rate is higher for increasing (A) energy generation parameter. While a decreasing trend is seen for augmenting heat source (B) parameter.
- Shear stress near cylinder increases for an increase in energy generation parameter.
- Thermal and diffusion transfer rate is higher for increasing heat source/sink parameter.
- Inertial forces when applied highly reduces friction coefficient, thermal and mass rate of transfer.

References

1 Hashim, Aamir Hamid, Masood Khan, Umair Khan, *Phys Lett A*, 382(30) (2018) 1982.
2 Shah Z, Bonyah E, Islam S, Khan W, Ishaq M, *Heliyon*, 4(10) (2018) e00825.
3 Muhammad Imran Asjad, Muhammad Zahid, Mustafa Inc, Dumitru Baleanu, Bandar Almohsen, *Alexandria Eng J*, 61(11) (2022) 8715.
4 Kumar K A, Reddy J R, Sugunamma V, and Sandeep N, *Inter J Fluid Mech Res*, 46(5) (2019).
5 Megahed A M, *Int J Modern Phys C*, 31(01) (2020) 2050019.
6 Abbas A, Jeelani M B, Alnahdi A S, and Ilyas, A. (2022). *Processes*, 10(6) (2022).
7 Sreenivasulu P, Poornima T, Vasu B, Reddy Gorla, R S, & Bhaskar Reddy N, *J Appl Comput Mech*, *7*(2) (2021), 638.
8 Vinoth Kumar B , Poornima T , Sreenivasulu P ,Subba Rao A, *APL Mater*,12 (2024) 041106.
9 Pandikunta S, Vasu B,Tamalapakula P, & Bhaskar Reddy N, *J Comput Appl Res Mechl Eng,*10(1)(2020)85.
10 Sreenivasulu P, Rao G S, Poornima T, Reddy N B, & Job V M, *SN Appl Sci*, 2, (2020) 1.
11 Souayeh B, Reddy M G, Sreenivasulu, P Poornima T, Rahimi-Gorji M, & Alarifi I M, *J MolLiq*, 284 (2019)163.
12 Raju K V S, Reddy T S, Raju M C, Narayana P S, & Venkataramana S, *Ain Shams Engineering Journal*, 5(2), (2014) 543.
13 Kho Y B, Hussanan A, Mohamed M K A, Sarif N M, Ismail Z, & Salleh M Z, *J Phys Conf. Ser,* **890** 012034 (2017).
14 Kumar K G, Rudraswamy N G, Gireesha B J, & Manjunatha S, *Results Phys*, *7* (2017) 3196.
15 Megahed M A, *J Egypt Math Soc*, 27(1) (2019) 12.
16 Ramamoorthy M, & PallavarapuL, *Heat Transfer*, 49 (8) (2020)4410.
17 Saravana R, Hemadri Reddy R, Narasimha Murthy K V, & Makinde O D. *Heat Transfer*, 51(4) (2022) 3187.
18 HamdanM H, Silva-Zea R, Erazo-Bone R, Chuchuca-Aguilar F, & Escobar-Segovia K, *J Appl Math Phy*, 8(10) (2020) 2115.
19 Geindreau, Christian &Auriault, Jean-Louis, *J Fluid Mech*, 466 (343) (2020).
20 Acharya A K, Dash G C, Mishra S R, *Phys Res Int*, 8 (2014).
21 Krishna M V, Jyothi K & Chamkha A J, *J Porous Media*, 23 (8) (2020) 751.
22 Raghunath K, Obulesu M & Sivaprasad R, *AIP Conf. Proc.,* 2220 (2020)130003.
23 Mishra SR, Hoque M M, Mohanty B & Anika NN, *Nonlinear Eng*, 8 (1) (2019) 65.
24 Sreenivasulu P, Poornima T, Reddy N B & Reddy M G, *J Nanofluids*, 8 (5) (2019) 1076.
25 Sreenivasulu P, Bhaskar ReddyN & Poornima T, *Front Heat Mass Transf*, 9(1) (2017) 1.
26 Poornima T, Sreenivasulu P & Souayeh B, *Int J Ambient Energy*, 44 (1) (2023) 2469.
27 Konda & Jayarami Reddy, *Multidiscip Model Mater and Struct*, 15(2) (2019) 452.
28 Jyotshna M & Dhanalaxmi V, *European J Math Stat*, 3(5) (2022) 16.
29 Ying-Qing Song, Aamir Hamid, Tian-Chuan Sun, Ijaz Khan M, Sumaira Qayyum, Naveen Kumar R, Prasanna kumara B C, Sami Ullah Khan & Ronnason Chinram, *Alex Eng J*, 61(1) 2022 195.
30 Swain K, Sampada Kumar P& Dash G C, Trans Tech Publications, 389 (2018) 110.
31 RaoA S, PrasadV R, Bég O A, RashidiM, *J Porous Media* , 21(3) (2018) 279.
32 Prasad V R, Rao A S & Bég O A, *Theor Appl Mech* ,41(1) (2014) 37-70.
33 Keller H B, *Annu Rev Fluid Mech* ,10(1) (1978) 417.